



# Realization of laser intensity over $10^{23}$ W/cm<sup>2</sup>

JIN WOO YOON,<sup>1,2,†</sup> YEONG GYU KIM,<sup>1,3,†</sup> IL WOO CHOI,<sup>1,2</sup> JAE HEE SUNG,<sup>1,2</sup>  
HWANG WOON LEE,<sup>1</sup> SEONG KU LEE,<sup>1,2,4</sup> AND CHANG HEE NAM<sup>1,3,5</sup>

<sup>1</sup>Center for Relativistic Laser Science, Institute for Basic Science, 123 Cheomdangwagi-ro, Buk-gu, Gwangju 61005, Republic of Korea

<sup>2</sup>Advanced Photonics Research Institute, Gwangju Institute of Science and Technology, 123 Cheomdangwagi-ro, Buk-gu, Gwangju 61005, Republic of Korea

<sup>3</sup>Department of Physics and Photon Science, Gwangju Institute of Science and Technology, 123 Cheomdangwagi-ro, Buk-gu, Gwangju 61005, Republic of Korea

<sup>4</sup>e-mail: lsk@gist.ac.kr

<sup>5</sup>e-mail: chnam@gist.ac.kr

Received 21 January 2021; revised 18 March 2021; accepted 23 March 2021 (Doc. ID 420520); published 6 May 2021

**High-intensity lasers are critical for the exploration of strong field quantum electrodynamics. We report here a demonstration of laser intensity exceeding  $10^{23}$  W/cm<sup>2</sup> with the CoReLS petawatt (PW) laser. After wavefront correction and tight focusing with a two-stage adaptive optical system and an  $f/1.1$  ( $f = 300$  mm) off-axis parabolic mirror, we obtained near diffraction-limited focusing with a spot size of  $1.1 \mu\text{m}$  (FWHM). From the measurement of 80 consecutive laser shots at 0.1 Hz, we achieved a peak intensity of  $(1.1 \pm 0.2) \times 10^{23}$  W/cm<sup>2</sup>, verifying the applicability of the ultrahigh intensity PW laser for ultrahigh intensity laser–matter interactions. From the statistical analysis of the PW laser shots, we identified that the intensity fluctuation originated from air turbulence in the laser beam path and beam pointing. Our achievement could accelerate the study of strong field quantum electrodynamics by enabling exploration of nonlinear Compton scattering and Breit–Wheeler pair production.** © 2021 Optical Society of America under the terms of the OSA Open Access Publishing Agreement

<https://doi.org/10.1364/OPTICA.420520>

## 1. INTRODUCTION

With the development of ultrashort, high-power lasers based on the chirped pulse amplification technique [1], strong field physics has steadily advanced. In laser–matter interactions, a focused laser intensity is a key parameter governing the physical processes of strong field phenomena. In recent years, ultrahigh-power lasers with output over one petawatt have been constructed or are being developed in a few institutes around the world [2–10]. Laser intensity over  $10^{22}$  W/cm<sup>2</sup> was obtained with several petawatt class lasers, such as the HERCULES laser [11,12], the Texas Petawatt Laser [13], the J-KAREN-P laser [14], and the SULF laser [15], while the record high intensity of  $5 \times 10^{22}$  W/cm<sup>2</sup> was achieved with the CoReLS petawatt laser [16]. For further enhancement of laser intensity, ultrahigh-power laser facilities, such as Apollon [17], ELI [18], EP-OPAL [19], and SEL [20], with outputs of 10 PW and beyond, are under construction. With the development of ultrahigh-intensity lasers, investigations of electron acceleration, ion acceleration, and x-/γ-ray generation have been actively pursued [21–25].

For the exploration of strong field quantum electrodynamics (SFQED), ultrahigh-power lasers with intensity exceeding  $10^{23}$  W/cm<sup>2</sup> are strongly desired [26,27]. At this intensity level, SFQED phenomena will become accessible in the strongly nonlinear regime; ultra-intense gamma rays can be emitted via the nonlinear Compton scattering (NCS) and electron–positron pairs can be created via the nonlinear Breit–Wheeler process [28–31]. In

addition, proton acceleration can be dominated by radiation pressure acceleration (RPA) [32,33]. To realize laser intensity exceeding  $10^{23}$  W/cm<sup>2</sup>, we have developed a series of laser technologies necessary to obtain the highest laser intensity attainable and applied them to the CoReLS 4-PW laser.

In this work, we report the realization of laser intensity over  $10^{23}$  W/cm<sup>2</sup> by tightly focusing the CoReLS PW laser with an  $f/1.1$  off-axis parabolic mirror (OAP;  $f = 300$  mm) after correcting the wavefront with two-stage deformable mirrors. We statistically analyzed the wavefront fluctuation and the intensity stability of 80 consecutive PW laser shots at 0.1 Hz. The intensity stability is critical to achieve reproducible and consistent experimental results for investigations of high-field science.

## 2. EXPERIMENTAL METHODS

For the realization of the laser intensity over  $10^{23}$  W/cm<sup>2</sup>, we carefully carried out wavefront control of the PW laser. The layout of the CoReLS 4-PW laser and the experimental setup to control the wavefront and to measure the intensity are given in Fig. 1. The proper wavefront control is crucial to achieve near-diffraction-limited focusing of the PW laser. The wavefront of the PW laser was controlled at two positions: one before the pulse compressor and the other at the target chamber. The first deformable mirror (DM1, AKA Optics SAS, Marseille, France) was used to make

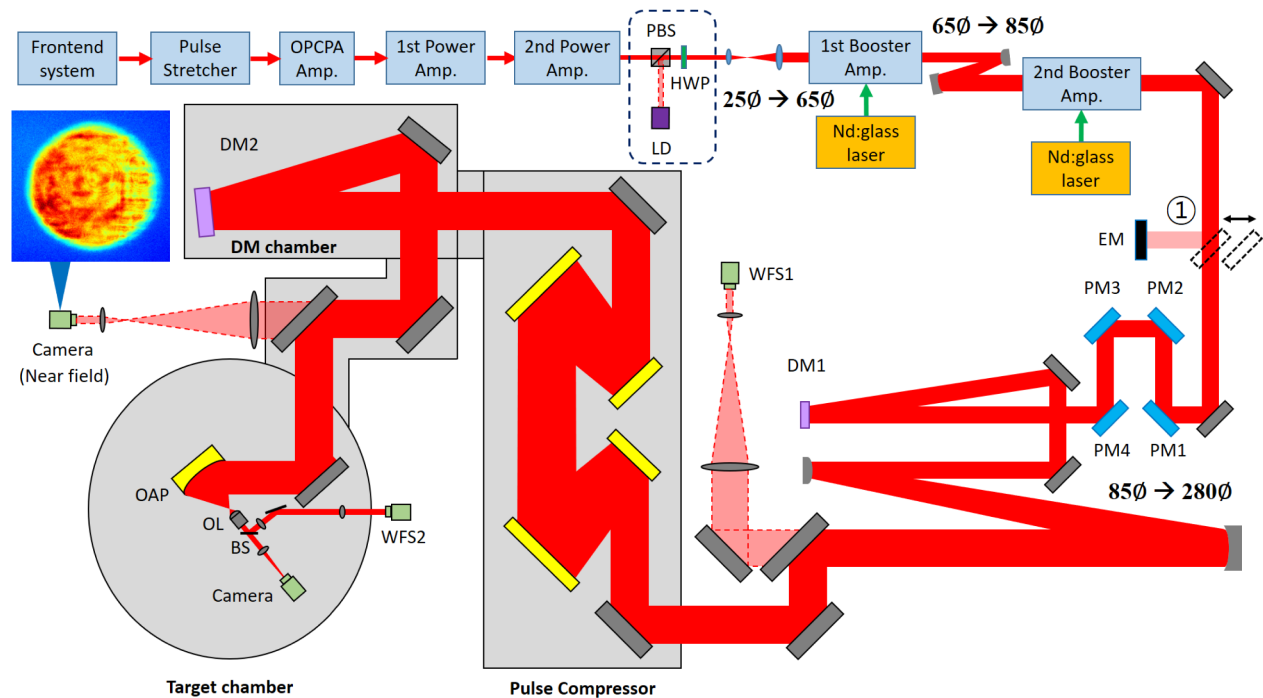


**Fig. 1.** Layout of the CoReLS petawatt laser and the experimental setup to achieve the laser intensity over  $10^{23}$  W/cm<sup>2</sup>. LD, laser diode; PBS, polarizing beam splitter; HWP, half-wave plate; EM, energy meter; PM1-4, partial reflection mirrors; DM1-2, deformable mirrors; WFS1-2, wavefront sensors; OAP,  $f/1.1$  off-axis parabolic mirror; OL, objective lens; and BS, beam splitter.

the wavefront flat before the pulse compressor, because the distorted wavefront can result in the spatiotemporal coupling during pulse compression that eventually degrades the focusing quality at the target chamber [8,34]. For wavefront control with DM1, a leakage beam through a reflection mirror, right after the final beam expander, was sent to a Shack–Hartmann wavefront sensor (WFS1, AKA Optics) via an imaging system including a large-aperture aspheric lens with a diameter of 300 mm ( $f = 1650$  mm). The wavefront aberration before the compressor was measured with WFS1 and fed back to a closed-loop system to control the DM1 with 100 mm diameter. The closed-loop was operated with low-energy laser pulses at 5 Hz without pumping booster amplifiers, and the laser energy was attenuated by a partial reflection mirror (PM1) with 1% reflectivity. After the closed-loop operation, DM1 voltages were fixed to the optimized values. It was reported that thermal loading to the compressor could induce wavefront distortion in the case of Pyrex gratings [35]. However, such an effect is minimal in the CoReLS PW laser with the compression gratings made of fused silica and the operation less than 0.1 Hz.

The wavefront aberration induced by the large-aperture optics, including the focusing OAP, after the pulse compressor was corrected using the second deformable mirror (DM2, AKA Optics). DM2 with 310 mm diameter and 127 actuators fully covers the laser beam. Right before the target chamber, the near-field beam profile was monitored with a leakage beam through a reflection mirror. The diagnostic setup and the measured beam profile are shown in Fig. 1. In the target chamber, the petawatt laser beam was tightly focused with an  $f/1.1$  OAP (300 mm effective focal length, 60° off-axis angle, Aperture Optical Sciences Inc., Meriden, CT, USA). Since the focal spot shape is very sensitive to the OAP alignment in the tight focusing configuration, we used an OAP mount with high precision (1  $\mu$ m for translation

and 5  $\mu$ rad for rotation) six-axis (three translational and three rotational) movements. To characterize the tight focusing with the OAP, the focused laser beam was collimated by a 50 $\times$  apochromatic objective lens ( $f = 4.0$  mm, Mitutoyo Corp., Kawasaki, Japan) and divided into two beams by a beam splitter for far-field imaging and wavefront measurement. The transmitted laser beam through the beam splitter was focused by an achromatic doublet ( $f = 125$  mm) and its far-field image was recorded with a 12-bit CMOS camera (SV10M6, 1.67  $\mu$ m pixel, EPIX, Inc., Buffalo Grove, IL, USA) in vacuum. At the same time, the reflected laser beam from the beam splitter was imaged onto a Shack–Hartmann wavefront sensor (WFS2, AKA Optics) via a pair of achromatic doublets ( $f = 200$  mm and  $f = 750$  mm) for the wavefront characterization.

The wavefront information measured with WFS2 was fed back to the closed-loop system connected with DM2 to compensate for the wavefront errors at the target area. DM voltages were optimized through the closed-loop operation initially running with low-energy laser pulses at 5 Hz without pumping booster amplifiers. After this preliminary operation of DM2, the wavefront and the focal spots were measured at the target chamber while pumping the booster amplifiers. When measuring the wavefront and the focal spot of the full power laser beam, the laser energy was attenuated by four partial reflection mirrors (PM1-4) with 1%, 1%, 1%, and 5% reflection coating (total reflectivity of  $5 \times 10^{-8}$ ). To avoid wavefront distortions due to the PMs, we used high-quality PMs with a surface flatness below 20 nm (rms). When a full-power beam was delivered to the target chamber for laser–matter interaction experiments, PMs were replaced with high-reflection mirrors with a flatness below 20 nm (rms) and the beam alignment was precisely checked by several beam pointing (near- and far-field) monitoring systems to ensure the same laser alignment.

In addition, a laser diode (LD) was installed right after the second power amplifier, as shown in the dotted box of Fig. 1. The LD beam was used as a stable light source to measure environmental effects on the wavefront fluctuations of the PW laser beamline before the pulse compressor using WFS1.

### 3. EXPERIMENTAL RESULTS

#### A. Optimization of Wavefront and Focal Spot

To achieve a near-diffraction-limited focal spot, we performed the wavefront correction of the petawatt laser and measured the focal spot image focused with the  $f/1.1$  OAP. The wavefronts measured with WFS2 before and after the correction are shown in Figs. 2(a) and 2(b). The WFS1 and WFS2 have a lenslet array with  $80 \times 80$  microlenses and provide wavefront maps reconstructed with 24 Zernike polynomials. After the wavefront correction, an almost flat wavefront was obtained and the rms wavefront error was successfully reduced from  $0.32 \mu\text{m}$  to  $0.05 \mu\text{m}$ . The focal spot images before and after the wavefront correction are shown in Figs. 3(a) and 3(b). After the correction, the focal spot image became a circular shape with a size of  $1.1 \mu\text{m}$  (FWHM). Figure 3(c) shows the ideal focal spot image calculated by the vectorial simulation with a monochromatic light ( $\lambda = 800 \text{ nm}$ ). The calculated ideal focal spot shows a slightly elliptical beam profile with the size (FWHM) of  $0.92 \text{ (H)} \times 0.89 \text{ (V)} \mu\text{m}^2$  due to the vector feature under the tight focusing [36]; it becomes a slightly smaller and circular shape of  $0.89 \text{ (H)} \times 0.89 \text{ (V)} \mu\text{m}^2$  without the vector feature. The focal spot deformation by the vector feature, however, cannot appear in the imaging camera due to the large  $f$ -number ( $f/30$ ,  $f = 125 \text{ mm}$ ) of the imaging system, and thus the actual focal spot area might be slightly larger than the measured one by 3%.

#### B. Peak Intensity Measurement

After the focal spot optimization, we obtained the peak intensity from the measured pulse energy, pulse shape, and focal spot shape by separately handling the temporal and spatial components of the spatiotemporal profile. Since both a near-diffraction-limited focal spot and near-Fourier-transform-limited pulse shape were obtained in this work, the spatiotemporal coupling might be insignificant. For more rigorous spatiotemporal characterization, we have developed a single-shot spatiotemporal characterization device and measured the spatiotemporal profile of the CoReLS PW laser pulse. Further details of the spatiotemporal coupling effect are given in Supplement 1, Section 1.

The temporal pulse shape was measured with a full aperture beam right after the pulse compressor. The full aperture beam was down-collimated to a  $3.5 \text{ mm}$  diameter with a spherical focusing mirror with  $f = 12,000 \text{ mm}$  and an OAP with  $f = 150 \text{ mm}$ .

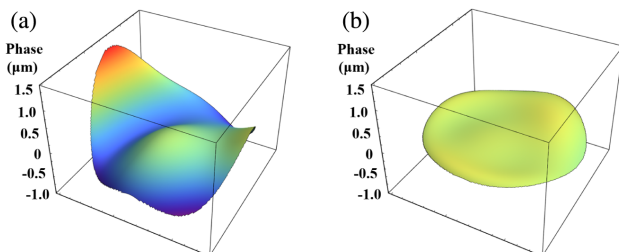


**Fig. 2.** Wavefront maps measured at the target chamber with WFS2: (a) before the wavefront correction (PV:  $2.11 \mu\text{m}$ , RMS:  $0.32 \mu\text{m}$ ) and (b) after the wavefront correction (PV:  $0.30 \mu\text{m}$ , RMS:  $0.05 \mu\text{m}$ ).

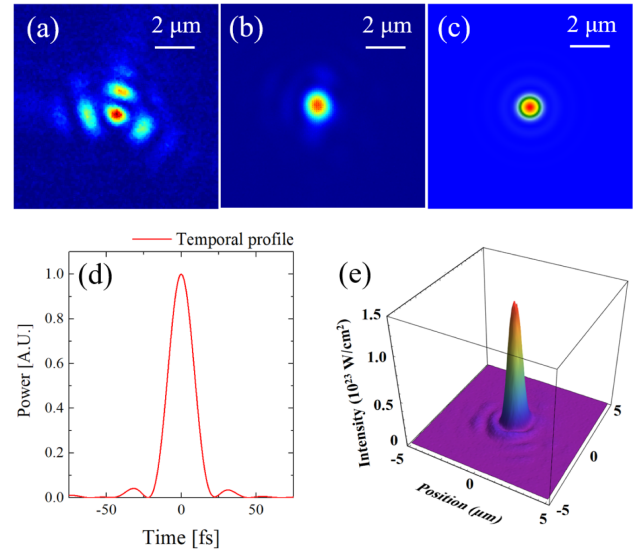


**Fig. 3.** Focal spot images measured at the target chamber: (a) before and (b) after the wavefront correction; (c) ideal focal spot image for the focusing with  $f/1.1$  OAP; (d) measured temporal profile ( $\tau_{1/2} = 19.6 \text{ fs}$  (FWHM)); and (e) 3D image of the focal spot for the case of the highest measured laser intensity.

Then the pulse shape was measured with a spectral phase interferometry for direct electric-field reconstruction (SPIDER) technique (FC-Spider, APE, Berlin, Germany). The measured pulse duration (FWHM,  $\tau_{1/2}$ ) was  $19.6 \pm 0.5 \text{ fs}$ , which is close to the transform-limited duration of  $19.0 \text{ fs}$ , as shown in Fig. 3(d). The peak power ( $P_0$ ) in the temporal domain was calculated using [14]

$$P_0 = E_0 / \tau_{\text{eff}} = E_0 / \int p(t) dt, \quad (1)$$

where  $\tau_{\text{eff}}$  is an effective pulse width and  $p(t)$  is a normalized optical power profile based on the temporal profile.

For the energy measurement, we used a pyroelectric sensor (PE80BF-DIF-C, Ophir-Spiricon, LLC, North Logan, UT, USA), and measured transmission efficiency of a laser beam before the final beam expander (position ① in Fig. 1) to the target position without pumping booster amplifiers, while high reflection mirrors were used instead of PMs. Amplified energy ( $E_a$ ) with pumping the booster amplifiers was measured at the position ① with a 20% reflection mirror, and then on-target Energy ( $E_0$ ) was estimated with the transmission efficiency. In the case of the full energy operation of the CoReLS petawatt laser,  $E_0$  was  $83 \text{ J}$ , obtained by compressing a laser pulse with  $E_a = 112 \text{ J}$  with a transmission efficiency of 74%. In this work,  $E_0$  was reduced to  $55.6 \pm 1.2 \text{ J}$  due to a decrease in the pump energy of the booster amplifiers ( $E_a = 89.7 \pm 2.0 \text{ J}$ ) and a reduction in the transmission efficiency of the pulse compressor (62%). From  $E_0 = 55.6 \text{ J}$  and the measured pulse profile in Fig. 3(d), the peak power ( $P_0$ ) of  $2.7 \text{ PW}$  was obtained from Eq. (1).

Then, the peak intensity ( $I_0$ ) was calculated from the measured peak power and the focal spot profile using [14]

$$I_0 = E_0 / (\tau_{\text{eff}} A_{\text{eff}}) = P_0 / A_{\text{eff}} = P_0 / \int i(x, y) dx dy, \quad (2)$$

where  $A_{\text{eff}}$  is an effective spot area and  $i(x, y)$  is the normalized intensity distribution of a measured focal spot. Using the measured

peak power, we obtained the peak intensity of  $1.4 \times 10^{23} \text{ W/cm}^2$  from the focal spot image in Fig. 3(b), which, to the best of our knowledge, is the first demonstration of the intensity exceeding  $10^{23} \text{ W/cm}^2$ . Figure 3(e) shows the 3D focal spot image for the case of the highest measured intensity. Here, by correcting the wavefront and tight focusing of PW laser pulses, we could successfully obtain the unprecedented laser intensity over  $10^{23} \text{ W/cm}^2$ , but the consistent generation of laser pulses with such intensity must be confirmed.

### C. Stability of the Wavefront and Intensity

Since the intensity stability at the focus is critical in the exploration of ultrahigh intensity laser-matter interactions, we examined the shot-to-shot variation of wavefront and intensity. For the inspection of wavefront stability, we measured the wavefront map of 80 consecutive shots of the petawatt laser operating at 0.1 Hz after the feedback correction of the wavefront with the DMs. In Fig. 4(a), the rms wavefront aberrations ( $\phi_{\text{RMS}}$ ) of 80 consecutive shots measured with WFS2 are shown, where the average and the standard deviation (SD) are  $0.079 \mu\text{m}$  and  $0.017 \mu\text{m}$ , respectively. The source of the fluctuations is discussed later. The Strehl ratio (SR), defined as the ratio of the peak intensity of a measured focal spot to the peak intensity of an ideal diffraction-limited focal spot, is an effective parameter to describe the focusability of a laser beam. We calculated the SR from the measured rms wavefront errors ( $\phi_{\text{RMS}}$ ) using the formula,  $\text{SR} \simeq \exp[-(2\pi\phi_{\text{RMS}}/\lambda)^2]$  [37]. The shot-to-shot SR variation is shown in Fig. 4(b) for the 80 consecutive shots, where the average SR is 0.68 and the fluctuation is 0.11 (SD).

For the statistical characterization of the intensity, the focal spot image of a wavefront corrected PW pulse was recorded and analyzed for 80 consecutive shots. Figure 4(c) shows the FWHM focal spot size ( $d_{\text{FWHM}} = \sqrt{d_x d_y}$ ) and the effective focal spot diameter ( $d_{\text{eff}} = 2\sqrt{A_{\text{eff}}/\pi}$ )

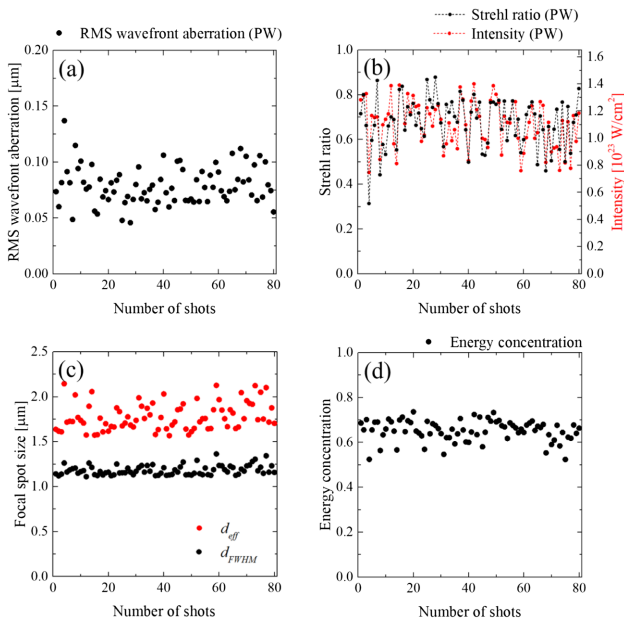


**Fig. 4.** (a) The rms wavefront error of the PW laser measured with WFS2 for 80 consecutive shots at 0.1 Hz and (b) corresponding Strehl ratio (black dot) and the peak intensity (red dot) obtained from the measured focal spot. (c) FWHM focal spot size ( $d_{\text{FWHM}} = \sqrt{d_x d_y}$ , black dot) and the effective focal spot diameter ( $d_{\text{eff}} = 2\sqrt{A_{\text{eff}}/\pi}$ , red dot), and (d) energy concentration within the first minimum for 80 consecutive shots of the PW laser focused with  $f/1.1$  OAP.

( $d_{\text{eff}} = 2\sqrt{A_{\text{eff}}/\pi}$ ), where  $d_x$  and  $d_y$  are the horizontal and the vertical focal spot sizes (FWHM), respectively. Figure 4(d) shows the energy concentration (EC) within the first minimum of a focal spot image. The measured FWHM focal spot size was  $1.2 \pm 0.1 \mu\text{m}$ , close to the diffraction limit of  $0.90 \mu\text{m}$ , the effective focal spot size was  $1.8 \pm 0.2 \mu\text{m}$ , and the energy concentration was  $0.65 \pm 0.05$ .

From the measured focal spots, we obtained the peak intensity for the 80 consecutive shots using Eq. (2), as shown by the red dots in Fig. 4(b). The average peak intensity and SD were  $1.1 \times 10^{23} \text{ W/cm}^2$  and  $0.2 \times 10^{23} \text{ W/cm}^2$  (16%), respectively. This result confirmed that we could obtain the laser intensity over  $10^{23} \text{ W/cm}^2$  on average. Here, we note that  $\Delta I_0/I_0 = \Delta A_{\text{eff}}/A_{\text{eff}} = 16\%$  on the assumption of constant energy and pulse width. Because the variation of laser energy ( $\Delta E_0/E_0 = 2.2\%$ ) and that of pulse width ( $\Delta \tau_{1/2}/\tau_{1/2} = 2.5\%$ ) are much smaller than the focal area variation ( $\Delta A_{\text{eff}}/A_{\text{eff}} = 16\%$ ), the intensity fluctuation was contributed mainly from the focal area variation, according to  $\Delta I_0/I_0 = \sqrt{(\Delta E_0/E_0)^2 + (\Delta \tau_{\text{eff}}/\tau_{\text{eff}})^2 + (\Delta A_{\text{eff}}/A_{\text{eff}})^2} \simeq 16\%$ . In addition, Fig. 4(b) shows that the shot-to-shot variation of the peak intensity (red dots) and that of the Strehl ratio (black dots) change quite consistently, which implies that the focal spot is affected mainly by the wavefront aberration. Thus, the intensity stability was affected primarily by the wavefront fluctuation that significantly influences the focal spot profile. Additionally, the shot-to-shot variation of the Strehl ratio does not exactly coincide with that of the intensity in Fig. 4(b), because the accuracy of the wavefront data at the beam edge was limited due to the cropped edge by the circular pupil of the wavefront sensor [14].

Considering the importance of wavefront fluctuation in intensity stability, we investigated the source of the wavefront fluctuation. In the case of tight focusing with a small  $f$ -number OAP, the wavefront of a focused beam is very sensitive to the alignment and even beam pointing. Since a small  $f$ -number OAP ( $f/1.1$ ) was used in this work, the wavefront fluctuation induced by the beam pointing might be significant. We estimated the wavefront fluctuation by analyzing the beam pointing of 80 consecutive shots, as shown in Fig. 5(a) where the horizontal and the vertical pointing variations (SD) are  $3.0 \mu\text{rad}$  and  $3.6 \mu\text{rad}$ , respectively. We also calculated the wavefront aberration, induced by the horizontal and the vertical pointings, with the ray-tracing tool, CODE V, for the experimental conditions that a laser beam with a diameter of  $280 \text{ mm}$  at  $800 \text{ nm}$  was focused by the OAP with  $f/1.1$ . According to the calculation,  $0^\circ$  and  $45^\circ$  astigmatisms were primarily induced by the beam pointing, and other aberration terms were negligible. Fluctuations (SD) of  $0^\circ$  and  $45^\circ$  astigmatisms calculated from the measured beam pointing data were  $0.052 \mu\text{m}$  and  $0.063 \mu\text{m}$ , respectively. We could then estimate the Strehl ratio using the induced astigmatisms for each laser shot, assuming that the laser had no aberration before the OAP. The calculated SR was  $0.94 \pm 0.06$ , as shown in Fig. 5(b); it indicates that beam pointing can be one of the possible sources of the wavefront fluctuation and the SR degradation at the target area.

To identify other causes of the wavefront fluctuation, we investigated the environmental effect on the wavefront fluctuation using a laser diode (LD) beam with a stable wavefront, installed right after the second power amplifier, as shown in Fig. 1. To rule out the laser amplification effects, the LD beam was used as a probe beam without pumping of two booster amplifiers. Because the main laser beam propagated in the air up to the pulse compressor, the effect

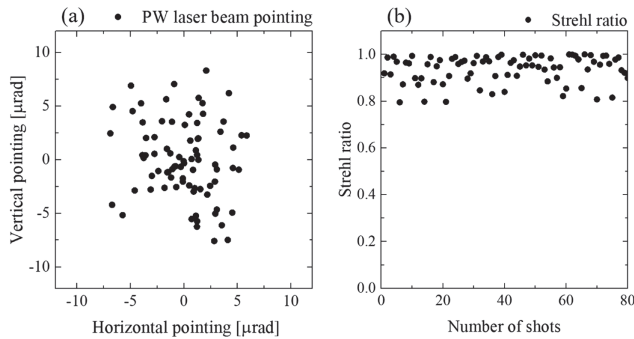


**Fig. 5.** (a) Beam pointing measured from 80 shots of the PW laser. (b) Variation of Strehl ratio induced by the beam pointing estimated for the case of ideal incident beams with flat wavefront.

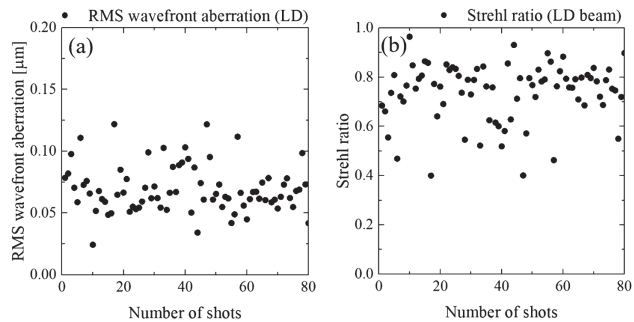


**Fig. 6.** (a) The rms wavefront error of an LD beam measured with WFS1 for 80 shots and (b) the corresponding Strehl ratio.

**Table 1. Strehl Ratio of the PW Beam and the LD Beam, and the Beam Pointing Effects on the Strehl Ratio (calculation)**

	Strehl Ratio
PW beam	$0.68 \pm 0.11$
LD beam	$0.74 \pm 0.08$
Beam pointing effects (calculation)	$0.94 \pm 0.06$

of air turbulence on wavefront fluctuation must be investigated. To measure the air turbulence effect, the wavefront fluctuation of the LD beam during the propagation in the air was measured with WFS1 right before the vacuum compressor chamber in the absence of the main laser beam. The rms wavefront aberration of the LD beam measured at 0.1 Hz was  $0.071 \pm 0.017 \mu\text{m}$ , as shown in Fig. 6(a), and the corresponding Strehl ratio calculated from the measured wavefront aberration was  $0.74 \pm 0.08$ , as shown in Fig. 6(b). Compared to the fluctuations of the wavefront and the Strehl ratio of the PW laser beam in Figs. 4(a) and 4(b), the LD beam has a comparable level of wavefront fluctuation and Strehl ratio fluctuation, indicating that the air turbulence in the beam path before the compressor is the major contributor to the wavefront fluctuation of the PW laser. Table 1 shows a comparison of the Strehl ratio of the PW laser beam and the LD beam, and beam pointing effects on the Strehl ratio. These results show that the intensity stability of the petawatt laser can be improved further by suppressing the air turbulence in the laser beam path as well as the beam pointing.

## 4. CONCLUSION

To realize ultrahigh intensity over  $10^{23} \text{ W/cm}^2$ , we carried out a wavefront correction and tight focusing of the CoReLS petawatt laser. After the wavefront correction using a two-stage DM system and the tight focusing with an  $f/1.1$  OAP ( $f = 300 \text{ mm}$ ), near-diffraction-limited focusing was achieved. The average and the variation of peak laser intensity at the focus were  $1.1 \times 10^{23} \text{ W/cm}^2$  and  $0.2 \times 10^{23} \text{ W/cm}^2$ , respectively, which, to the best of our knowledge, is the first realization of laser intensity over  $10^{23} \text{ W/cm}^2$ . It was found that the focused intensity fluctuation was caused by the wavefront fluctuation due to the air turbulence in the beam path and the beam pointing. With the PW laser of an intensity over  $10^{23} \text{ W/cm}^2$ , we plan to explore strong field QED phenomena, such as the nonlinear Compton scattering and the nonlinear Breit–Wheeler processes, and proton/ion acceleration dominated by the RPA mechanism.

**Funding.** Institute for Basic Science (IBS-R012-D1); Ultrashort Quantum Beam Facility (UQBF) operation program (140011) through Advanced Photonics Research Institute, Gwangju Institute of Science and Technology.

**Acknowledgment.** The authors thank Jeong Moon Yang, Yeon Joo Son, Seung Yeon Kim, Han Bum Lim, Dongyoon Yoo, Tae Yoon Kim, and Jong Eun Lee for technical assistance.

**Disclosures.** The authors declare no conflicts of interest.

**Data Availability.** Data underlying the results presented in this paper are not publicly available at this time but may be obtained from the corresponding authors upon reasonable request.

**Supplemental document.** See Supplement 1 for supporting content.

<sup>†</sup>These authors contributed equally to this paper.

## REFERENCES

1. D. Strickland and G. Mourou, "Compression of amplified chirped optical pulses," *Opt. Commun.* **55**, 447–449 (1985).
2. C. N. Danson, C. Haefner, J. Bromage, T. Butcher, J.-C. F. Chanteloup, E. A. Chowdhury, A. Galvanauskas, L. A. Gizzi, J. Hein, D. I. Hiller, N. W. Hopps, Y. Kato, E. A. Khazanov, R. Kodama, G. Korn, R. Li, Y. Li, J. Limpert, J. Ma, C. H. Nam, D. Neely, D. Papadopoulos, R. R. Penman, L. Qian, J. J. Rocca, A. A. Shaykin, C. W. Siders, C. Spindloe, S. Szatmári, R. M. G. M. Trines, J. Zhu, P. Zhu, and J. D. Zuegel, "Petawatt and exawatt class lasers worldwide," *High Power Laser Sci. Eng.* **7**, e54 (2019).
3. C. Danson, P. Brummitt, R. Clarke, J. Collier, B. Fell, A. Frackiewicz, S. Hancock, S. Hawkes, C. Hernandez-Gomez, P. Holligan, M. Hutchinson, A. Kidd, W. Lester, I. Musgrave, D. Neely, D. Neville, P. Norreys, D. Pepler, C. Reason, W. Shaikh, T. Winstone, R. Wyatt, and B. Wyborn, "Vulcan Petawatt—an ultra-high-intensity interaction facility," *Nucl. Fusion* **44**, S239–S246 (2004).
4. G. Xu, T. Wang, Z. Li, Y. Dai, Z. Lin, Y. Gu, and J. Zhu, "1 kJ petawatt laser system for SG-II-U program," *Rev. Laser Eng.* **36**, 1172–1175 (2008).
5. E. W. Gaul, M. Martinez, J. Blakeney, A. Jochmann, M. Ringuette, D. Hammond, T. Borger, R. Escamilla, S. Douglas, W. Henderson, G. Dyer, A. Erlandson, R. Cross, J. Caird, C. Ebberts, and T. Ditmire, "Demonstration of a 1.1 petawatt laser based on a hybrid optical parametric chirped pulse amplification/mixed Nd:glass amplifier," *Appl. Opt.* **49**, 1676–1681 (2010).
6. J. H. Sung, S. K. Lee, T. J. Yu, T. M. Jeong, and J. Lee, "0.1 Hz 1.0 PW Ti:sapphire laser," *Opt. Lett.* **35**, 3021–3023 (2010).
7. C. Liu, S. Banerjee, J. Zhang, S. Chen, K. Brown, J. Mills, N. Powers, B. Zhao, G. Golovin, I. Ghebregziabher, and D. Umstadter, "Repetitive petawatt-class laser with near-diffraction-limited focal spot and transform-limited pulse duration," *Proc. SPIE* **8599**, 859919 (2013).
8. J. H. Sung, H. W. Lee, J. Y. Yoo, J. W. Yoon, C. W. Lee, J. M. Yang, Y. J. Son, Y. H. Jang, S. K. Lee, and C. H. Nam, "4.2 PW, 20 fs Ti:sapphire laser at 0.1 Hz," *Opt. Lett.* **42**, 2058–2061 (2017).

9. Z. Gan, L. Yu, S. Li, C. Wang, X. Liang, Y. Liu, W. Li, Z. Guo, Z. Fan, X. Yuan, L. Xu, Z. Liu, Y. Xu, J. Lu, H. Lu, D. Yin, Y. Leng, R. Li, and Z. Xu, "200 J high efficiency Ti:sapphire chirped pulse amplifier pumped by temporal dual-pulse," *Opt. Express* **25**, 5169–5178 (2017).
10. K. Nakamura, H. Mao, A. J. Gonsalves, H. Vincenti, D. E. Mittelberger, J. Daniels, A. Magana, C. Toth, and W. P. Leemans, "Diagnostics, control and performance parameters for the BELLA high repetition rate petawatt class laser," *IEEE J. Quantum Electron.* **53**, 1–21 (2017).
11. S.-W. Bahk, P. Rousseau, T. A. Planchon, V. Chvykov, G. Kalintchenko, A. Maksimchuk, G. A. Mourou, and V. Yanovsky, "Generation and characterization of the highest laser intensities ( $10^{22}$  W/cm<sup>2</sup>)," *Opt. Lett.* **29**, 2837–2839 (2004).
12. V. Yanovsky, V. Chvykov, G. Kalinchenko, P. Rousseau, T. Planchon, T. Matsuoka, A. Maksimchuk, J. Nees, G. Cheriaux, G. Mourou, and K. Krushelnick, "Ultra-high intensity-300-TW laser at 0.1 Hz repetition rate," *Opt. Express* **16**, 2109–2114 (2008).
13. G. Tiwari, E. Gaul, M. Martinez, G. Dyer, J. Gordon, M. Spinks, T. Toncian, B. Bowers, X. Jiao, R. Kupfer, L. Lisi, E. McCary, R. Roycroft, A. Yandow, G. D. Glenn, M. Donovan, T. Ditmire, and B. M. Hegelich, "Beam distortion effects upon focusing an ultrashort petawatt laser pulse to greater than  $10^{22}$  W/cm<sup>2</sup>," *Opt. Lett.* **44**, 2764–2767 (2019).
14. A. S. Pirozhkov, Y. Fukuda, M. Nishiuchi, H. Kiriya, A. Sagisaka, K. Ogura, M. Mori, M. Kishimoto, H. Sakaki, N. P. Dover, K. Kondo, N. Nakanii, K. Huang, M. Kanasaki, K. Kondo, and M. Kando, "Approaching the diffraction-limited, bandwidth-limited petawatt," *Opt. Express* **25**, 20486–20501 (2017).
15. Z. Guo, L. Yu, J. Wang, C. Wang, Y. Liu, Z. Gan, W. Li, Y. Leng, X. Liang, and R. Li, "Improvement of the focusing ability by double deformable mirrors for 10-PW-level Ti: sapphire chirped pulse amplification laser system," *Opt. Express* **26**, 26776–26786 (2018).
16. J. W. Yoon, C. Jeon, J. Shin, S. K. Lee, H. W. Lee, I. W. Choi, H. T. Kim, J. H. Sung, and C. H. Nam, "Achieving the laser intensity of  $5.5 \times 10^{22}$  W/cm<sup>2</sup> with a wavefront-corrected multi-pw laser," *Opt. Express* **27**, 20412–20420 (2019).
17. J. Zou, C. Le Blanc, D. Papadopoulos, G. Chériaux, P. Georges, G. Mennerat, F. Druon, L. Lecherbourg, A. Pellegrina, P. Ramirez, F. Giambro, A. Fréneau, F. Leconte, D. Badarau, J. Boudenne, D. Fournet, T. Valloton, J. Paillard, J. Veray, M. Pina, P. Monot, J. Chambaret, P. Martin, F. Mathieu, P. Audebert, and F. Amiranoff, "Design and current progress of the Apollon 10 PW project," *High Power Laser Sci. Eng.* **3**, e2 (2015).
18. S. Gales, K. A. Tanaka, D. L. Balabanski, F. Negoita, D. Stutman, O. Tesileanu, C. A. Ur, D. Ursescu, I. Andrei, S. Ataman, M. O. Cernaianu, L. D'Alessi, I. Dancus, B. Diaconescu, N. Djourelou, D. Filipescu, P. Ghenuche, D. G. Ghita, C. Matei, K. Seto, M. Zeng, and N. V. Zamfir, "The extreme light infrastructure—nuclear physics (ELI-NP) facility: new horizons in physics with 10 PW ultra-intense lasers and 20 MeV brilliant gamma beams," *Rep. Prog. Phys.* **81**, 094301 (2018).
19. J. Bromage, S.-W. Bahk, I. A. Begishev, C. Dorrer, M. J. Guardalben, B. N. Hoffman, J. Oliver, R. G. Roides, E. M. Schiesser, M. J. Shoup, III, M. Spilatro, B. Webb, D. Weiner, and J. D. Zuegel, "Technology development for ultraintense all-OPCPA systems," *High Power Laser Sci. Eng.* **7**, e4 (2019).
20. E. Cartlidge, "The light fantastic," *Science* **359**, 382–385 (2018).
21. D. Margarone, O. Klimo, I. J. Kim, J. Prokūpek, J. Limpouch, T. M. Jeong, T. Mocek, J. Pšikal, H. T. Kim, J. Proška, K. H. Nam, L. Štolcová, I. W. Choi, S. K. Lee, J. H. Sung, T. J. Yu, and G. Korn, "Laser-driven proton acceleration enhancement by nanostructured foils," *Phys. Rev. Lett.* **109**, 234801 (2012).
22. C. G. R. Geddes, C. Toth, J. van Tilborg, E. Esarey, C. B. Schroeder, D. Bruhwiler, C. Nieter, J. Cary, and W. P. Leemans, "High-quality electron beams from a laser wakefield accelerator using plasma-channel guiding," *Nature* **431**, 538–541 (2004).
23. M. Mirzaie, S. Li, M. Zeng, N. A. M. Hafz, M. Chen, G. Y. Li, Q. J. Zhu, H. Liao, T. Sokollik, F. Liu, Y. Y. Ma, L. M. Chen, Z. M. Sheng, and J. Zhang, "Demonstration of self-truncated ionization injection for GeV electron beams," *Sci. Rep.* **5**, 14659 (2015).
24. N. D. Powers, I. Ghebregziabher, G. Golovin, C. Liu, S. Chen, S. Banerjee, J. Zhang, and D. P. Umstadter, "Quasi-monoenergetic and tunable X-rays from a laser-driven Compton light source," *Nat. Photonics* **8**, 28–31 (2014).
25. G. Sarri, D. Corvan, W. Schumaker, J. Cole, A. Di Piazza, H. Ahmed, C. Harvey, C. Keitel, K. Krushelnick, S. Mangles, Z. Najmudin, D. Symes, A. Thomas, M. Yeung, Z. Zhao, and M. Zepf, "Ultrahigh brilliance multi-MeV  $\gamma$ -ray beams from nonlinear relativistic Thomson scattering," *Phys. Rev. Lett.* **113**, 224801 (2014).
26. T. G. Blackburn, "Radiation reaction in electron-beam interactions with high-intensity lasers," *Rev. Mod. Plasma Phys.* **4**, 5 (2020).
27. H. Vincenti, "Achieving extreme light intensities using optically curved relativistic plasma mirrors," *Phys. Rev. Lett.* **123**, 105001 (2019).
28. J. Jiao, B. Zhang, J. Yu, Z. Zhang, Y. Yan, S. He, Z. Deng, J. Teng, W. Hong, and Y. Gu, "Generating high-yield positrons and relativistic collisionless shocks by 10 PW laser," *Laser Part. Beams* **35**, 234–240 (2017).
29. M. Marklund and P. K. Shukla, "Nonlinear collective effects in photon-photon and photon-plasma interactions," *Rev. Mod. Phys.* **78**, 591–640 (2006).
30. A. Di Piazza, C. Müller, K. Z. Hatsagortsyan, and C. H. Keitel, "Extremely high-intensity laser interactions with fundamental quantum systems," *Rev. Mod. Phys.* **84**, 1177–1228 (2012).
31. M. Vranic, O. Klimo, G. Korn, and S. Weber, "Multi-GeV electron-positron beam generation from laser-electron scattering," *Sci. Rep.* **8**, 4702 (2018).
32. S. S. Bulanov, E. Esarey, C. B. Schroeder, S. V. Bulanov, T. Z. Esirkepov, M. Kando, F. Pegoraro, and W. P. Leemans, "Radiation pressure acceleration: the factors limiting maximum attainable ion energy," *Phys. Plasmas* **23**, 056703 (2016).
33. J. Domański, J. Badziak, and M. Marchwiany, "Laser-driven acceleration of heavy ions at ultra-relativistic laser intensity," *Laser Part. Beams* **36**, 507–512 (2018).
34. M. Miranda, M. Kotur, P. Rudawski, C. Guo, A. Harth, A. L'Huilier, and C. L. Arnold, "Spatiotemporal characterization of ultrashort laser pulses using spatially resolved Fourier transform spectrometry," *Opt. Lett.* **39**, 5142–5145 (2014).
35. V. Leroux, S. W. Jolly, M. Schnepf, T. Eichner, S. Jalas, M. Kirchen, P. Messner, C. Werle, P. Winkler, and A. R. Maier, "Wavefront degradation of a 200 TW laser from heat-induced deformation of in-vacuum compressor gratings," *Opt. Express* **26**, 13061–13071 (2018).
36. T. M. Jeong, S. Weber, B. L. Garrec, D. Margarone, T. Mocek, and G. Korn, "Spatio-temporal modification of femtosecond focal spot under tight focusing condition," *Opt. Express* **23**, 11641–11656 (2015).
37. V. Mahajan, "Strehl ratio for primary aberrations in terms of their aberration variance," *J. Opt. Soc. Am.* **73**, 860–861 (1983).